Fluctuating Flow of Thermomicropolar Fluid
Past a Vertical Surface

Md. M. Hossain, A. C. Mandal, N. C. Roy, and M. A. Hossain
Department of Mathematics,
University of Dhaka, Bangladesh
anwar@univdhaka.edu

Abstract

The unsteady free convection boundary layer flow of a thermo-micropolar fluid along a vertical plate has been investigated in this paper. The temperature of the plate is assumed to be oscillating about a mean temperature, $\theta_w(x)$, with small amplitude ε. The governing boundary layer equations are analyzed using straight forward finite difference method. The effects of the material parameters such as micropolar heat conduction parameter, N^*, the vortex viscosity parameter, K, on the shear stress, τ_ω, surface heat transfer, q_ω, and the couple-stress, m_ω, have been investigated.

Keywords: Thermomicropolar fluid, fluctuating surface temperature, micropolar heat conduction

MSC 2010 No.: 76D, 80A

1. Introduction

Free convection has been the focus of many researchers due to its numerous applications in heat transfer such as: rocket nozzles, cooling of nuclear reactors, high speed aircrafts and their atmospheric re-entry, high sinks in turbine blades, chemical devices and process equipment, formation and dispersion of fog, distribution of temperature and moisture over agricultural fields and groves of fruit trees, damage of crops due to freezing and pollution of the environment etc.

Hence a thorough investigation and knowledge of heat transfer process must be acquired in order to be able to design heat exchangers, bearing etc., so that no overheating or damage is caused to the components. In case of heated vertical plate the heat transferred from the surface causes a decrease in liquid density and a subsequent upward flow due to buoyancy force occurs. Mathur (1970) has studied the free convection flow of an elastico-viscous fluid past a non-uniformly heated vertical plate. An excellent survey of this problem for Newtonian and non-Newtonian fluids has been given in Mathur (1970). Although a number of studies on the laminar free convection flow and heat transfer of Newtonian and non-Newtonian fluids have been found in literature, these do not give satisfactory results if the fluid is a mixture of heterogeneous means such as liquid crystals, ferro-liquid, liquid with polymer additives, which is more realistic and important from technological point of view.

For the realistic description of the flow of fluids such as fluids with polymeric additives etc., the classical continuum mechanics cannot be used. To overcome this, Eringen (1966) has introduced the concept of thermomicropolar fluids that deals with a class of fluids, which exhibit certain microscopic effects arising from the local structure and micromotions of the fluid elements. These fluids contain dilute suspensions of rigid micromolecules with individual motions, which support stress and body moments and are influenced by spin-inertia. The theory of micropolar fluid and its extension to thermomicropolar fluids Eringen (1972) may form suitable non-Newtonian fluid models which can be used to analyze the behavior of exotic lubricants (Khonsari and Brewe (1989) and Hadimoto and Tokioka (1969)), colloidal suspensions or polymeric fluids (Lockwood et al. (1987)), liquid crystals (Lockwood et al. (1987) and Lee and Eringen (1971)), and animal blood (Ariman et al. (1973)). Kolpashchikov et al. (1983) have developed a method to measure micropolar parameters experimentally. A thorough review of this subject and application of micropolar fluid mechanics has been provided by Ariman et al. (1973) and Ahmadi (1976).

Jena and Mathur (1981) studied the similarity solutions for the steady laminar free convection boundary layer flow of a thermomicropolar fluid past a non-isothermal vertical flat plate. Hossain et al. (1999) investigated a steady two-dimensional natural convection flow of a viscous incompressible thermomicropolar fluid with uniform spin-gradient over a flat plate with a small inclination to the horizontal. Studies of heat convection in micropolar fluids have been focused on flat plates (Jena and Mathur (1981, 1982), Gorla (1983); Yucel (1989); Hossain et al. (1995); Chiu and Chou (1993)) and a wavy surface (Muri (1961)). Gorla and Takhar (1991) examined the effect of buoyancy force on an unsteady incompressible micropolar fluid in the vicinity of the lower stagnation point of a circular cylinder. Helmy (2000) studied the unsteady free convection flow of a micropolar fluid for a vertical plate under uniform heating after solving the governing equations using the state space and Laplace-transform techniques.

Mixed and natural convection flow of micropolar fluids with uniform surface temperature/surface heat flux has been studied along a solid surface by Chang and Lee (2008), stretching sheet by Ishak et al. (2008), a truncated cone by Postelnicu (1012); effect of melting heat transfer on the stagnation flow along stretched or shrinked surface investigated by Takob et al. (2008). Cheng (2008, 2010) considered conjugate effect thermal and mass diffusion on the flow of thermo-micropolar fluid. On the above flows effect of transverse magnetic has been considered by, Aziz (2006), Eshak et al. (2008), Yakob and Ishak (2011). In addition to the

above studies, attention has been given to see effect of radiation on the flow of thermo-microplar fluid by Ishak (2010), Hsiao (2010), Bhattacharyyaa, et al. (2012) and Zheng (2012). All the above studies are restricted to similarity flows in the boundary layer region. Recently, Saleem et al. (2011) has investigated the natural convection flow of micropolar fluid in a rectangular cavity heated from below with cold sidewalls and Mahfouz (2013) the buoyancy driven micropolar fluid flow within uniformly heated eccentric annulus.

It is worth mentioning that unsteady laminar boundary layer theory, one area of study which has received much attention in the past deals with boundary layer responses to imposed oscillations. Lighthill (1954) was the first to have studied the unsteady forced flow of a viscous incompressible fluid past a flat plate and a circular cylinder with small amplitude oscillation in free stream. The corresponding problem of unsteady free convection flow along a vertical plate with oscillating surface temperature was studied by Nanda and Sharma (1963) and Eshghy et al. (1965). In consideration of this class of problems, Muhuri and Maiti (1967) and Verma (1982) analyzed the effect of oscillation of the surface temperature on the unsteady free convection along a horizontal plate.

All the above investigations are based on the assumption that the surface temperature oscillates with small amplitude about the uniform mean temperature and they were carried out employing the Karman-Pohlhausen approximate integral method. Based on the linearized theory, Kelleher and Yang (1968) have studied the heat transfer responses of a laminar free convection boundary layer along a vertical heated plate to surface temperature oscillations, when the mean surface temperature $Tw(x)$ is proportional to x^n, where x is the distance measured from the leading edge of the plate. This study had been extended by Hossain et al. (1998 a, b) for magnetohydrodynamic flows for variable mean surface temperature and surface heat flux. Recent investigation on fluctuating hydro-magnetic natural convection flow of an optically gray fluid past a magnetized vertical surface with effect of thermal radiation has been made by Ashraf et al. (2012). On the other hand, Jaman et al. (1012) extend the problem posed by Kelleher and Yang (1968) for the case of the flow along a circular cylinder.

In this study, the unsteady free convection boundary layer flow of a thermomicropolar fluid along a vertical plate has been investigated considering that the surface temperature is oscillating about a mean temperature $\theta_w(x)$ with a small amplitude ε as posed by Kelleher and Yang (1968). As for as known, this problem has not been discussed in the literature.

2. Mathematical Formalisms

A two-dimensional unsteady laminar boundary layer flow of a thermo-micropolar fluid along a permeable vertical flat plate is considered. The temperature of the ambient fluid and the surface are assumed to be T_∞ and T_W respectively. The co-ordinate system and the flow configuration are shown in Figure 1.
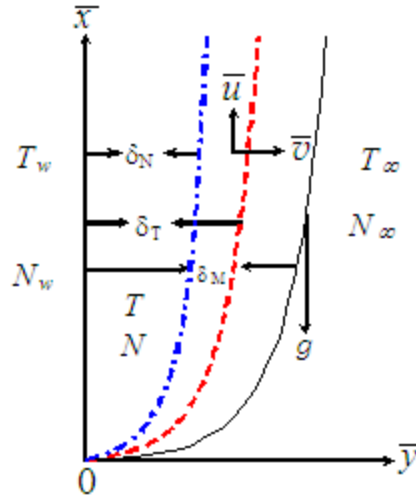
Figure 1. Flow Configuration and Coordinate System

Under the usual Boussinesq approximation the dimensionless equations of conservation of mass, momentum, angular velocity and energy that govern the flow are given as (see Jena and Mathur (1981)),

$$\frac{\partial u}{\partial x}+\frac{\partial v}{\partial y}=0,$$

(1)

$$\frac{\partial u}{\partial t}+u\frac{\partial u}{\partial x}+v\frac{\partial u}{\partial y}=\left(1+K\right)\frac{\partial^2 u}{\partial y^2}+K\frac{\partial N}{\partial y}+\theta,$$

(2)

$$\frac{\partial N}{\partial t}+u\frac{\partial N}{\partial x}+v\frac{\partial N}{\partial y}=\left(1+\frac{K}{2}\right)\frac{\partial^2 N}{\partial y^2}-K\left(2N+\frac{\partial u}{\partial y}\right),$$

(3)

$$\frac{\partial \theta}{\partial t}+u\frac{\partial \theta}{\partial x}+v\frac{\partial \theta}{\partial y}=\frac{1}{\text{Pr}}\frac{\partial^2 \theta}{\partial y^2}+N^*\left(\frac{\partial \theta}{\partial x}\frac{\partial N}{\partial y}-\frac{\partial \theta}{\partial y}\frac{\partial N}{\partial x}\right),$$

(4)

which are based on the following dimensionless dependent and independent variables

$$x=\frac{\overline{x}}{L},\ \ y=\frac{\overline{y}}{L},\ \ \overline{u}=\frac{v}{L}u,\ \ \overline{v}=\frac{v}{L}v,$$

$$\overline{N}=\frac{v}{L^2}N,\ \ t=\frac{v}{L^2}\overline{t},\ \ \theta=\frac{g\beta\left(\overline{T}-\overline{T}_\infty\right)L^3}{v^2}.$$

(5)

Here, $\left(\overline{x},\overline{y}\right)$ are the co-ordinates parallel with and perpendicular to the flat surface respectively, $\left(\overline{u},\overline{v}\right)$ are the velocity components, t, time, $\overline{N}$, the angular velocity, θ, dimensionless

temperature, j, the micro-inertia per unit mass, ρ, the density of the fluid, g the acceleration due to gravity, κ, the thermal conductivity of the fluid, $\gamma = (\mu + \kappa/2)j$, the gyro-viscosity coefficient and α^*, the micropolar heat conduction coefficient.

Following Jena and Mathur (1981), it is assumed that micro-inertia, j, is a constant and, therefore, it is set equal to a reference value, $j_0 = L^2$. Further, L is the characteristic length, $K = (\kappa/\mu)$ is vortex viscosity parameter, μ, the dynamic viscosity, $Pr = (\nu/\alpha)$ is the Prandtl number that gives the ratio of momentum diffusivity to thermal diffusivity, ν, viscosity coefficient, $N^* = (\alpha^*/L^2)$ is the micropolar heat conduction parameter and ε is the amplitude of oscillation.

The corresponding boundary conditions are

$$u = 0, \quad v = 0, \quad N = -n\frac{\partial u}{\partial y}, \quad \theta = \theta_w(x)(1 + \varepsilon \cos(\tau)) \quad \text{at} \quad y = 0, \tag{6}$$

$$u = 0, \quad \theta = 0 \quad \text{as} \quad y \to \infty, \tag{7}$$

where n is a constant such that $0 \le n \le 1$. The case $n = 0$ corresponds to the strong concentration of microelements. Thus equation (6) suggests that when $n = 0$ (i.e., $N = 0$) near the walls, the concentration of the particles is strong enough so that the micro-elements near the walls are unable to rotate because of its concentration. The case, $n = 1/2$, on the other hand, indicates the vanishing of anti-symmetric part of the stress tensor and denotes weak concentration.

The boundary condition for $\theta(\tau, 0)$ given in (6)–(7) suggests the solutions of equations (1)–(4) of the following form:

$$u = u_0 + \varepsilon \exp(i\tau)u_1, \tag{8}$$

$$v = v_0 + \varepsilon \exp(i\tau)v_1, \tag{9}$$

$$N = N_0 + \varepsilon \exp(i\tau)N_1, \tag{10}$$

$$\theta = \theta_0 + \varepsilon \exp(i\tau)\theta_1, \tag{11}$$

where, $\omega t = \tau$. Further, u_0, v_0, N_0 and θ_0 represent the flow variables for the steady mean flow and u_1, v_1, N_1 and θ_1 are the fluctuating flow variables. The real parts of the functions defined in (8)–(11) are our desired solutions.

Now, substituting the functions given in (8)–(11) into equations (1)–(7) and equating the terms up to $O(\varepsilon)$, one gets

$$\frac{\partial u_0}{\partial x} + \frac{\partial v_0}{\partial y} = 0, \tag{12}$$

$$u_0 \frac{\partial u_0}{\partial x} + v_0 \frac{\partial u_0}{\partial y} = (1+K)\frac{\partial^2 u_0}{\partial y^2} + K\frac{\partial N_0}{\partial y} + \theta_0, \tag{13}$$

$$u_0 \frac{\partial N_0}{\partial x} + v_0 \frac{\partial N_0}{\partial y} = \left(1+\frac{K}{2}\right)\frac{\partial^2 N_0}{\partial y^2} - K\left(2N_0 + \frac{\partial u_0}{\partial y}\right), \tag{14}$$

$$u_0 \frac{\partial \theta_0}{\partial x} + v_0 \frac{\partial \theta_0}{\partial y} = \frac{1}{\Pr}\frac{\partial^2 \theta_0}{\partial y^2} + N^*\left(\frac{\partial \theta_0}{\partial x}\frac{\partial N_0}{\partial y} - \frac{\partial \theta_0}{\partial y}\frac{\partial N_0}{\partial x}\right), \tag{15}$$

with boundary conditions

$$u_0 = 0, \quad v_0 = 0, \quad N_0 = -n\frac{\partial u_0}{\partial y}, \quad \theta_0 = \theta_w(x) \quad \text{at} \quad y = 0, \tag{16}$$

$$u_0 = 0, \quad \theta_0 = 0 \quad \text{as} \quad y \to \infty_{.}, \tag{17}$$

and

$$\frac{\partial u_1}{\partial x} + \frac{\partial v_1}{\partial y} = 0, \tag{18}$$

$$iu_1 + u_0 \frac{\partial u_1}{\partial x} + u_1 \frac{\partial u_0}{\partial x} + v_0 \frac{\partial u_1}{\partial y} + v_1 \frac{\partial u_0}{\partial y} = (1+K)\frac{\partial^2 u_1}{\partial y^2} + K\frac{\partial N_1}{\partial y} + \theta_1, \tag{19}$$

$$iN_1 + u_0 \frac{\partial N_1}{\partial x} + u_1 \frac{\partial N_0}{\partial x} + v_0 \frac{\partial N_1}{\partial y} + v_1 \frac{\partial N_0}{\partial y} = \left(1+\frac{K}{2}\right)\frac{\partial^2 N_1}{\partial y^2} - K\left(2N_1 + \frac{\partial u_1}{\partial y}\right), \tag{20}$$

$$\begin{aligned} i\theta_1 + u_0 \frac{\partial \theta_1}{\partial x} &+ u_1 \frac{\partial \theta_0}{\partial x} + v_0 \frac{\partial \theta_1}{\partial y} + v_1 \frac{\partial \theta_0}{\partial y} \\ &= \frac{1}{\Pr}\frac{\partial^2 \theta_1}{\partial y^2} + N^*\left(\frac{\partial \theta_0}{\partial x}\frac{\partial N_1}{\partial y} + \frac{\partial \theta_1}{\partial x}\frac{\partial N_0}{\partial y} - \frac{\partial \theta_0}{\partial y}\frac{\partial N_1}{\partial x} - \frac{\partial \theta_1}{\partial y}\frac{\partial N_0}{\partial x}\right), \end{aligned} \tag{21}$$

subject to the boundary conditions

$$u_1 = 0, \; v_1 = 0, \; N_1 = -n\frac{\partial u_1}{\partial y}, \; \theta_1 = \theta_w(x) \quad \text{at} \quad y = 0, \tag{22}$$

and

$$u_1 \to 0, \; \theta_1 \to 0 \quad \text{as} \quad y \to \infty. \tag{23}$$

Here, the equations (12)–(17) are the equations for the steady state flow and those (18)–(23) are for the fluctuating flow.

3. Methods of Solution

In this section, emphasis is given to the method of solution which is used to solve the boundary layer equations (12)–(17) will represent the steady mean flow and those (18)–(23) the oscillating flow. The numerical solutions are obtained with the help of an efficient finite difference scheme.

To get the similarity equations for the steady state equations (12)–(17), we introduce the following group of transformations:

$$\psi_0 = xf(\eta), \; N_0 = xg(\eta), \; \theta_0 = x\Theta_0(\eta), \; \eta = y, \tag{24}$$

where ψ_0 is the stream function for the steady state flow defined by

$$u_0 = \frac{\partial \psi_0}{\partial \eta}, v_0 = -\frac{\partial \psi_0}{\partial x}. \tag{25}$$

Thus, we have

$$(1+K)f''' + ff'' - f'^2 + Kg' + \Theta_0 = 0, \tag{26}$$

$$\left(1 + \frac{K}{2}\right)g'' + fg' - f'g - K(f'' + 2g) = 0, \tag{27}$$

$$\frac{1}{\text{Pr}}\Theta_0'' + f\Theta_0' - f'\Theta_0 + N^*(\Theta_0 g' - \Theta_0' g) = 0. \tag{28}$$

The boundary conditions to be satisfied by the above equations are

$$f = 0, \; f' = 0, \; g = -nf'', \; \Theta_0 = 1 \text{ at } y \to 0, \tag{29}$$

$$f'(0) = 0, \; \Theta_0 = 0 \text{ at } y \to \infty. \tag{30}$$

Here, " ′ " denotes differentiation with respect to η.

Equations (26)–(28) are considered by Jena and Mathur (1981). Representative numerical values of shear stress, surface heat transfer and couple stress obtained from the present investigation of these equations are entered in Table 1, for comparison with those of Jena and Mathur (1981). From this table it is seen that the present solutions are in excellent agreement with those of Jena and Mathur (1981).

Table 1. The effect of variation of K on shear stress, surface heat transfer and couple-stress when $Pr = 9.0$ and $N^* = 1.0$

	$K = 0.1$			$K = 0.25$		
	$F''(0)$	$-G'(0)$	$-\theta'(0)$	$F''(0)$	$-G'(0)$	$-\theta'(0)$
Jena and Mathur (1981)	0.1558	-0.0365	0.3675	0.1480	-0.0389	0.3561
Present	0.15574	-0.03652	0.36764	0.14829	-0.03883	0.35787

Again, to get the similarity equations for the unsteady state equations (18)–(23), we introduce the following group of transformations:

$$\psi_1 = xF(\eta), \ N_1 = xG(\eta), \ \theta_1 = x\Theta_1(\eta), \ \eta = y, \tag{31}$$

where ψ_1 is the stream function for the unsteady flow defined   by

$$u_1 = \frac{\partial \psi_1}{\partial \eta}, \quad v_1 = -\frac{\partial \psi_1}{\partial x}. \tag{32}$$

Thus, equations (19)–(21) then reduce to

$$iF' + 2f'F' - fF'' - f''F = (1+K)F''' + KG' + \Theta_1, \tag{33}$$

$$iG + f'G - fG' + F'g - Fg' = \left(1 + \frac{K}{2}\right)G'' - K(F'' + 2G), \tag{34}$$

$$i\Theta_1 + f'\Theta_1 - f\Theta_1' + F'\Theta_0 - F\Theta_0' = \frac{1}{Pr}\Theta_1'' + N^*\left(\Theta_0 G' + \Theta_1 g' - \Theta_0'G - \Theta_1'g\right), \tag{35}$$

and the boundary conditions become

$$F = 0, \ F' = 0, \ G = -nF'', \ \Theta_1 = 1 \quad \text{at} \ \ y = 0, \tag{36}$$

and

$$F \to 0, \ F' \to 0, \ \Theta_1 \to 0 \quad \text{as} \ \ y \to \infty. \tag{37}$$

The set of equations (26)–(28) and (33)–(35) together with the boundary conditions (29)–(30) and (36)–(37) can be integrated by straight forward finite difference method. Before going to apply the aforementioned method we first set $f = V_0$, $f' = U_0$, $F = V$ and $F' = U$ so that the equations (26)–(28) reduce to

$$(1+K)U_0'' + V_0 U_0' - (U_0)^2 + Kg' + \Theta_0 = 0, \tag{38}$$

$$\left(1 + \frac{K}{2}\right)g'' + V_0 g' - U_0 g - K\left(\frac{\partial U_0}{\partial \eta} + 2g\right) = 0, \tag{39}$$

$$\frac{1}{\text{Pr}}\Theta_0'' + V_0 \Theta_0' - U_0 \Theta_0 + N^*\left(\Theta_0 g' - \Theta_0' g\right) = 0. \tag{40}$$

with boundary conditions

$$V_0 = 0,\ U_0 = 0,\ g = -nU_0',\ \Theta_0 = 1 \quad \text{at}\ \ \eta = 0, \tag{41}$$

and

$$\tag{42}$$
$$U_0 = 0,\ \Theta_0 = 0\ \text{at}\ \eta \to \infty.$$

and the equations (33)–(35) take the form

$$iU + 2U_0 U - V_0 U' - VU_0' = (1+K)U'' + KG' + \Theta_1, \tag{43}$$

$$iG + GU_0' - VG' + U'g - Vg' = \left(1 + \frac{K}{2}\right)G'' - K(U' + 2G), \tag{44}$$

and

$$\tag{45}$$
$$i\Theta_1 + U_0'\Theta_1 - V\Theta_1' + U\Theta_0 - V\Theta_0' = \frac{1}{\text{Pr}}\Theta_1'' + N^*\left(\Theta_0 G' + \Theta_1 g' - \Theta_0' G - \Theta_1' g\right).$$

Now equations (38)–(40) are discretized by a simple numerical scheme, in which we use central-difference for diffusion terms and convection terms and thus, for example, (38) gives

$$\left\{\frac{1+K}{\Delta\eta^2} + \frac{(V_0)_j}{2\Delta\eta}\right\}(U_0)_{j+1} + \left\{\frac{1+K}{\Delta\eta^2} - \frac{(V_0)_j}{2\Delta\eta}\right\}(U_0)_{j-1} - \left\{\frac{2(1+K)}{\Delta\eta^2} - (U_0)_j\right\}(U_0)_j$$

$$\tag{46}$$

$$= -K\left(\frac{g_{j+1} - g_{j-1}}{2\Delta\eta}\right) - \Theta_j.$$

Equation (46) can be rewritten in the form

$$A_j \left(U_0 \right)_{j+1} + B_j \left(U_0 \right)_j + C_j \left(U_0 \right)_{j-1} = D_j,$$

(47)

where

$$A_j = \frac{1+K}{\Delta \eta^2} + \frac{\left(V_0 \right)_j}{2\Delta \eta}, \quad B_j = -\left\{ \frac{2(1+K)}{\Delta \eta^2} - \left(U_0 \right)_j \right\}, \quad C_j = \frac{1+K}{\Delta \eta^2} - \frac{\left(V_0 \right)_j}{2\Delta \eta},$$

and

$$D_j = -K \left(\frac{g_{j+1} - g_{j-1}}{2\Delta \eta} \right) - \Theta_j.$$

Similarly, the equations (39)–(40) can be rendered in the form (47). The resulted tri-diagonal algebraic system is solved by Gaussian elimination technique. The computation is started at $\eta = 0$, and then marches downstream implicitly. The ordinary differential equations governing the upstream condition at $\eta = 0$ can be obtained by taking the limit of equations (46) that η approaches zero. The associated boundary conditions are equations (41)–(42) with $\eta = 0$.

Now we define the functions

$$U = U_r + iU_i, \quad \Theta_1 = \Theta_r + i\Theta_i, \quad G = G_r + iG_i.$$

(48)

Using (48) into (43)–(45) and then separating the real and imaginary parts, we can solve the resulting systems of equations employing the procedure described above.

Again, from the set of relations (8)–(11) together with the transformations given in (24)–(25) and (31)–(32), we get the expression for the dimensionless axial velocity, temperature and angular velocity functions as given below

$$u(\tau,\eta)/x = f' + \varepsilon \left[\cos(\tau) U_r - \sin(\tau) U_i \right],$$

(49)

$$\theta(\tau,\eta)/x = \theta + \varepsilon \left[\cos(\tau) \Theta_r - \sin(\tau) \Theta_i \right],$$

(50)

$$N(\tau,\eta)/x = g + \varepsilon \left[\cos(\tau) G_r - \sin(\tau) G_i \right].$$

(51)

In equations (38)–(40), U_r, Θ_r, G_r and U_i, Θ_i, G_i are respectively, the real and imaginary parts of the velocity function, $u_1(\tau,\eta)$, the temperature function, $\Theta_1(\tau,\eta)$ and angular velocity, $G(\tau,\eta)$.

From the application point of view, it is needed to interpret the behavior of physical quantities such as surface shear stress, τ_ω, surface heat flux, q_ω, and the surface couple stress, m_ω, which may be obtained from the following dimensionless relations

$$\bar{\tau} = \left[(\mu+k)\left(\frac{\partial \bar{u}}{\partial \bar{y}}\right) + k\bar{N}\right]_{\bar{y}=0}, \quad \bar{q}_\omega = \left[-k\frac{\partial \bar{T}}{\partial \bar{y}} + \beta_c\frac{\partial \bar{N}}{\partial \bar{x}}\right]_{\bar{y}=0}, \quad \bar{m}_\omega = \left(\gamma\frac{\partial \bar{N}}{\partial \bar{y}} + \alpha_c\frac{\partial \bar{T}}{\partial \bar{x}}\right)_{\bar{y}=0}. \tag{52}$$

Using the equation (6) on equation (41) we obtain

$$\tau_\omega = (1+K)\left(\frac{\partial u}{\partial y}\right)_{y=0}, \quad q_\omega = -\left(\frac{\partial \theta}{\partial y}\right)_{y=0}, \quad m_\omega = \left(1+\frac{K}{2}\right)\left(\frac{\partial N}{\partial y}\right)_{y=0}, \tag{53}$$

where

$$\tau_\omega = \frac{L^2}{\nu}\bar{\tau}, \quad q_\omega = -\frac{g\beta L^4}{\kappa\nu^2}\bar{q}, \quad m_\omega = \frac{L^3}{\nu}\bar{m}$$

are, respectively, dimensionless surface shear stress, surface heat flux and the surface couple stress.

Once the solutions of the equations (26)–(28) and (33)–(37) are known, the values of the physical quantities are readily obtained. These are the shear stress, τ_ω, the rate of heat transfer, q_ω, and the couple-stress, m_ω, at the surface of the plate, which are important from the experimental point of view. Thus, we obtain

$$\tau_\omega = (1+K)x\left[\frac{\partial u_0}{\partial y} + \varepsilon A_u \cos(\tau+\phi_u)\right], \tag{54}$$

$$q_\omega = \frac{\partial \theta_0}{\partial y} + \varepsilon A_T \cos(\tau+\phi_T), \tag{55}$$

$$m_\omega = \left(1+\frac{K}{2}\right)\left[\frac{\partial N_0}{\partial y} + \varepsilon A_N \cos(\tau+\phi_N)\right], \tag{56}$$

where $\partial u_0/\partial y$, $\partial\theta_0/\partial y$ and $\partial N_0/\partial y$ are, respectively, the steady mean shear stress, surface heat transfer and couple stress.

Here, it is proposed to express the available solutions in terms of amplitude (A_u, A_T, A_N) and phase (ϕ_u, ϕ_T, ϕ_N) of the shear stress, the heat transfer rate and the couple-stress having the following relations:

$$A_u = \sqrt{\tau_r^2 + \tau_i^2}, \quad A_T = \sqrt{q_r^2 + q_i^2}, \quad A_N = \sqrt{m_r^2 + m_i^2} \tag{57}$$

and

$$\phi_u = \tan^{-1}\frac{\tau_i}{\tau_r}, \quad \phi_T = \tan^{-1}\frac{q_i}{q_r}, \quad \phi_N = \tan^{-1}\frac{m_i}{m_r}, \tag{58}$$

where the real parts of the transverse velocity gradient, temperature gradient, and couple-stress at the surface are τ_r, q_r and m_r respectively and the imaginary parts of those are τ_i, q_i and m_i respectively.

4. Results and Discussion

In this study, the straight forward finite difference method has been employed in finding the solutions of the equations governing the unsteady natural convection boundary layer flow of a viscous and incompressible fluid along a vertical plate. The results are expressed in terms of transient the shear stress, τ_ω, surface heat transfer, q_ω, and couple stress, m_ω, showing the effects of the physical parameters involved in the flow field, such as, the micropolar heat conduction parameter, N^*, and vortex viscosity parameter, K.

The effect of the vortex viscosity parameter, K, on the amplitude, A_u, and phase, ϕ_u, of the surface shear stress is presented in Figure 2(a) and 2(b) respectively. It is evident from the figures that the amplitude and phase of the shear stress decrease as the value of the vortex viscosity parameter, K, increases. This is expected because an increase in the value of the vortex viscosity parameter gives rise to the total viscosity of the fluid flow, which in turn lowers the magnitude of the amplitude and phase of the surface shear stress. Surface heat transfer is the major cause of such reduction in the above mentioned quantities. Thus, micropolar fluids exhibit drag reduction behavior compared to viscous fluids.
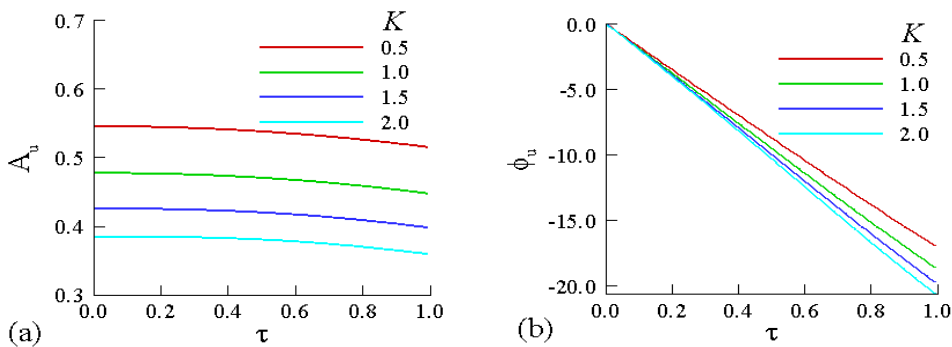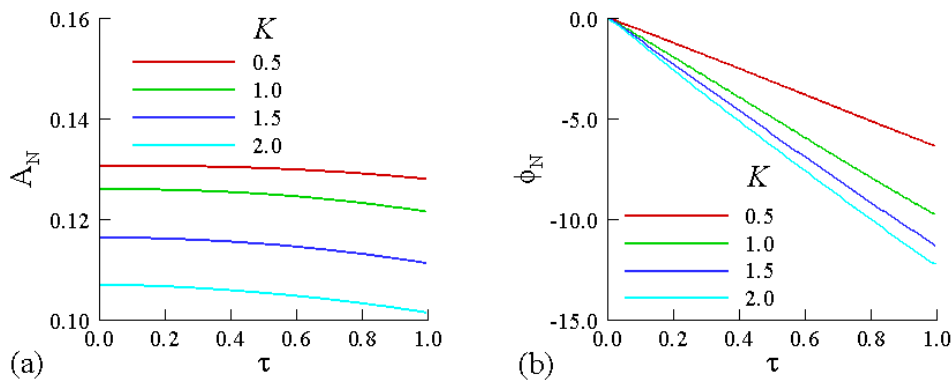

Figure 2. Amplitude and phase of the surface shear stress showing the effect of K when
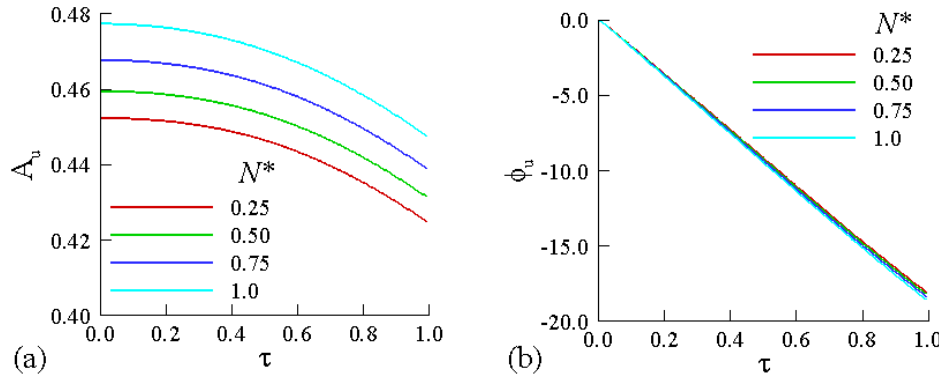$\varepsilon = 0.1, Pr = 9.0, N^* = 1.0$
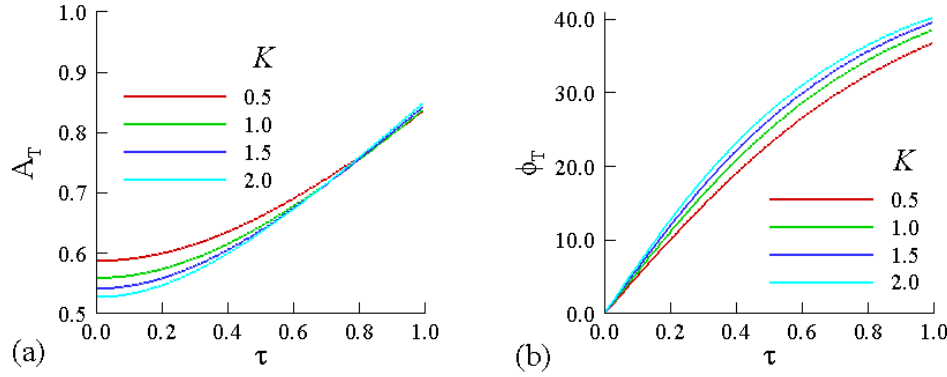
Figure 3. Amplitude and phase of the surface heat transfer showing the effect of K when
$\varepsilon = 0.1, \quad Pr = 9.0, N^* = 1.0$

Figures 3(a) and 3(b) depict the effect of the vortex viscosity parameter, K, on the amplitude, A_T, and phase, ϕ_T, of the surface heat transfer. From the figures, it is seen that the amplitude of the surface heat transfer decreases while the phase increases when the value of the vortex viscosity parameter, K, is increased. In this case, an increase in the vortex viscosity parameter leads to an increase in the rotation of microelements which decelerates the fluid flow and ultimately diminishes the amplitude of heat transfer. However, the phase of the heat transfer increases which is expected since total viscosity of the fluid increases as K gets stonger and due to fluid friction ϕ_T enhances within the boundary layer region.

The effect of varying the vortex viscosity parameter, K, on the amplitude, A_N, and phase, ϕ_N, of the couple stress is shown in Figure 4(a) and 4(b). We observe that the amplitude and phase of the couple stress decrease owing to the increase of the vortex viscosity parameter, K. Here again, an increase in the vortex viscosity parameter gives rise to the rotation of microelements which decelerates the motion of the fluid and ultimately diminishes the amplitude as well as phase of the couple stress.
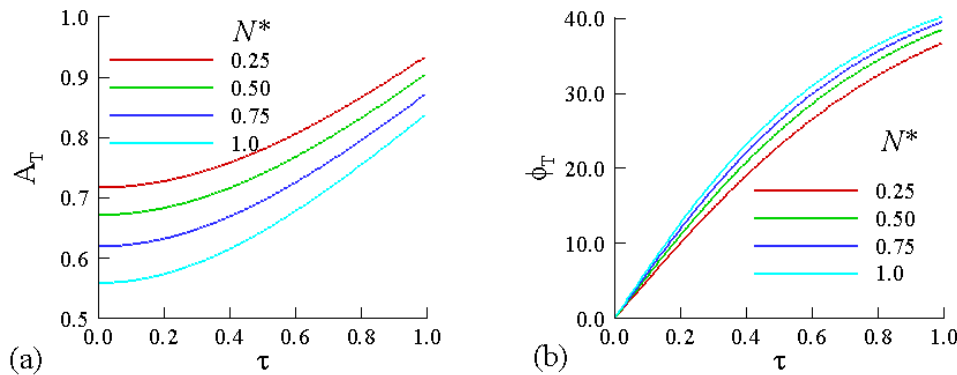

Figure 4. Amplitude and phases of the couple stress showing the effect of K when $\varepsilon = 0.1$,
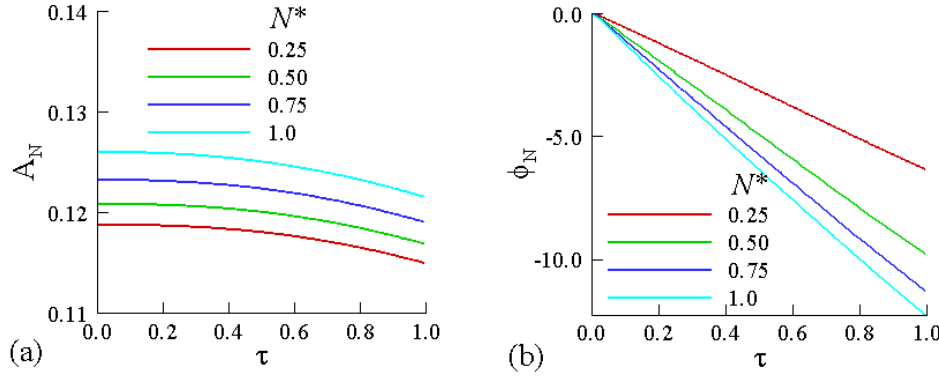$Pr = 9.0, N^* = 1.0$

Figure 5. Amplitude and phase of surface shear stress showing the effect of N^* when $\varepsilon = 0.1$,
$Pr = 9.0$, $N^*=1.0$

In Figure 5 the effect of micropolar heat conduction parameter, N^*, is shown for $N^* = 0.25$, 0.50, 0.75, 1.0 while other parameters are $\varepsilon = 0.1$ and $Pr = 9.0$. It is observed from this figure that the amplitude of the surface shear stress enhances due to the increase in the micropolar heat conduction parameter, N^*. However, the phase of the shear stress does not vary much but if we look closely it is anticipated that it slightly diminishes. This result is due to the fact that micropolar fluids offer a greater resistance (resulting from dynamic viscosity and vortex viscosity) to the fluid motion compared to Newtonian fluids.

The influence of micropolar heat conduction parameter, N^* ($= 0.25$, 0.50, 0.75, 1.0) on amplitude and phase of heat transfer is shown in Figure 6. It can be seen that the amplitude of heat transfer micropolar fluid decreases whereas the phase of heat transfer increases considerably. It happens because the rotation of microelements increases due to an increase in the micropolar heat conduction parameter which results in the decrease in the amplitude of heat transfer while phase of heat transfer increases.

Figure 6. Amplitude and phase of surface heat transfer showing the effect of N^* when
$\varepsilon = 0.1$, $Pr = 9.0$, $N^*=1.0$

Figure 7. Amplitude and phase of couple stress showing the effect of N^* when $\varepsilon = 0.1$, $Pr = 9.0$, $N^* = 1.0$

The effect of micropolar heat conduction parameter, N^*, on the amplitude and phase of couple stress is depicted in Figure 7. The physical parameters are set to be $N^* = 0.25$, 0.50, 0.75, 1.0, $\varepsilon = 0.1$ and $Pr = 9.0$. One can find that amplitude of the couple stress increases while phase decreases extensively when micropolar heat conduction parameter enhances from 0.25 to 1.0.

4.1. Effect of Micropolar Heat Conduction Parameter, N^* on Transient Shear Stress, Surface Heat Transfer and Couple Stress Coefficients

Attention is now given to see the effect of the micropolar heat conduction parameter $N^* (= 0.25, 0.50, 0.75, \text{ and } 1.0)$ on the transient shear stress, τ_ω, while $Pr = 9.0$. These figures display the effect of N^* on shear stress, τ_ω. As N^* increases, the shear stress, τ_ω, increases. In Figure 8(a), for every value of the heat conduction parameter N^*, there exists a local maximum of the shear stress, τ_ω. These maximum values of the shear stress, τ_ω, are recorded to be 0.66683, 0.68414, 0.70324, and 0.72449 at $\tau = 6.6$ for $N^* = 0.25$, 0.50, 0.75, and 1.0, respectively. For $\tau = 6.6$, the shear stress increases by 2.3%, 5.5% and 8.7%, respectively, as N^* increases from 0.25 to 0.50, 0.75 and 1.0. Figure 8(b) shows the surface heat transfer coefficient, q_ω, against τ for different values of the micropolar heat conduction parameter $N^* (= 0.25, 0.50, 0.75, \text{ and } 1.0)$ while $Pr = 9.0$. These figures display the effect of N^* on the heat transfer coefficient, q_ω.

As N^* increases, the surface heat transfer coefficient, q_ω, decreases. In the same figure, for all values of the heat conduction parameter N^*, there exists the local maximum of the surface heat transfer coefficient, q_ω, in each case. These maximum values of the surface heat transfer coefficient, q_ω, are seen to be 0.62630, 0.56880, 0.50547, and 0.43516 at $\tau = 5.7$ for $N^* = 0.25$, 0.50, 0.75, and 1.0, respectively. At $\tau = 5.7$, there are decreases in the heat transfer coefficient, q_ω, by 9.18, 21.24 and 30.51 percent respectively, as N^* increases from 0.25 to 0.50, 0.75 and 1.0. Figure 8(c) depicts the couple stress coefficient, m_ω, against τ for different values of the heat conduction parameter $N^* (= 0.25, 0.50, 0.75 \text{ and } 1.0)$ while $Pr = 9.0$. These figures display the effect of N^* on the couple stress coefficient, m_ω.

As N^* increases, the couple stress coefficient, m_ω, increases. This happens because the increase of N^* means that the heat conduction through the fluid increases so that the viscosity of the fluid decreases. Again Figure 8(c) shows that there exists a local maximum of the couple stress coefficient, m_ω, for every values of the heat conduction parameter, N^*. These maximum values of the couple stress coefficient, m_ω, are found to be 0.48063, 0.49328, 0.50724, and 0.52276 at $\tau =$

6.4 for $N^* = 0.25$, 0.50, 0.75, and 1.0, respectively. At $\tau = 6.4$, the shear stress increases by 2.63, 5.53 and 8.76 percent, respectively, as N^* increases from 0.25 to 0.50, 0.75 and 1.0.

Table 2. Amplitudes and phases of oscillation in shear stress, surface heat transfer and couple stress showing the effect of K when $\varepsilon = 0.1$, $Pr = 9.0$, $N^* = 1.0$

τ	A_u	A_T	A_N	ϕ_u	ϕ_T	ϕ_N
			$K = 0.5$			
0.0	0.54433	0.57995	0.13461	0.00000	0.00000	0.00000
0.1	0.54402	0.58307	0.13459	-1.73080	5.07365	-0.50783
0.2	0.54310	0.59256	0.13454	-3.51399	10.09909	-1.12000
0.3	0.54156	0.60811	0.13445	-5.29338	14.86849	-1.74020
0.5	0.53656	0.65521	0.13411	-8.83135	23.29560	-3.00369
0.6	0.53309	0.68538	0.13383	-10.58221	26.87041	-3.64218
0.7	0.52896	0.71900	0.13348	-12.31395	30.01566	-4.28100
0.8	0.52420	0.75541	0.13305	-14.02027	32.75422	-4.91669
0.9	0.51882	0.79401	0.13254	-15.69445	35.11944	-5.54549
1.0	0.51287	0.83427	0.13195	-17.32975	37.14912	-6.16341
			$K = 2.0$			
0.0	0.38492	0.52198	0.10949	0.00000	0.00000	0.00000
0.1	0.38482	0.52686	0.10944	-1.93426	6.47870	-1.11614
0.2	0.38443	0.54166	0.10923	-4.01690	12.74616	-2.43792
0.3	0.38362	0.56492	0.10890	-6.13324	18.41238	-3.73035
0.5	0.38015	0.63021	0.10794	-10.46187	-10.46187	-6.23926
0.6	0.37727	0.66951	0.10734	-12.64779	31.23695	-7.47043
0.7	0.37356	0.71188	0.10663	-14.82082	34.25848	-8.68800
0.8	0.36904	0.75649	0.10582	-16.95900	36.76954	-9.88685
0.9	0.36377	0.80265	0.10490	-19.04228	38.84107	-11.05924
1.0	0.35784	0.84976	0.10387	-21.05359	40.53872	-12.19679

4.2. Effect of Vortex Viscosity Parameter, *K*, on Transient Shear Stress, Surface Heat Transfer and Couple Stress Coefficients

The effect of the vortex viscosity parameter, K, on the transient shear stress, τ_ω, surface heat transfer coefficient, q_ω, and coefficient of couple stress, m_ω, are presented in Figure 9 and in Table 2. It is evident from the figures and Table 2 that the shear stress coefficient, surface heat transfer coefficient and coefficient of couple stress decreases due to an increase in the value of the vortex viscosity parameter, K. Figure 9(a) illustrates shear stress, τ_ω, against τ for different values of the vortex viscosity parameter K (= 0.5, 1.0, 1.5 and 2.0) while $Pr = 9.0$. These figures display the effect of K on shear stress, τ_ω. As K increases, the shear stress, τ_ω, decreases. In the same figure, for all values of the vortex viscosity parameter K, we observe a local maximum of the shear stress, τ_ω. These maximum values of the shear stress, τ_ω, are 0.84163, 0.72448, 0.63753, and 0.57104 at $\tau = 6.6$ for $K = 0.5$, 1.0, 1.5 and 2.0, respectively. At $\tau = 6.6$, the shear stress decreases by 13.91, 24.25 and 32.15 percent, respectively, when K increases from 0.50 to 1.0, 1.5 and 2.0. Figure 9(b) shows the effect of the surface heat transfer coefficient, q_ω, against τ for different values of the vortex viscosity parameter K (= 0.5, 1.0, 1.5, and 2.0) while $Pr = 9.0$. This figure displays the effect of K on the heat transfer coefficient, q_ω. As K increases, the surface heat transfer coefficient, q_ω decreases. Again in Figure 9(b), for all values of the vortex viscosity parameter, K, there is a local maximum of the heat transfer, q_ω. These maximum values

of the heat transfer coefficient, q_ω, are seen to be 0.44791, 0.43549, 0.42693, and 0.41999 at $\tau =$ 5.6 for $K = 0.50$, 1.0, 1.5 and 2.0, respectively. At $\tau = 5.6$, the surface heat transfer coefficient, q_ω, decreases by 2.77, 4.68 and 6.23 percent, respectively, as K increases from 0.50 to1.0, 1.50 and 2.0.

Finally Figure 9(c) depicts the couple stress coefficient, m_ω, against τ for different values of the vortex viscosity parameter K (= 0.5, 1.0, 1.5, and 2.0) while $Pr = 9.0$. This figure displays the effect of K on the couple stress coefficient, m_ω. With the increase of K, the couple stress coefficient, m_ω decreases. In the same Figure, for all values of the vortex viscosity parameter K, there exists a local maximum of the couple stress coefficient, m_ω. These maximum values of the couple stress coefficient, m_ω, are noticed to be 0.59832, 0.52276, 0.46347, and 0.41697 at $\tau = 6.4$ for $K = 0.50$, 1.0, 1.5, and 2.0 respectively. At $\tau = 6.4$, the shear stress decreases by 12.62, 22.53 and 30.30 percent, respectively, as K increases from 0.50 to 1.0, 1.5 and 2.0.

4.3. Effect of Micropolar Heat Conduction Parameter, N^* on Transient Velocity Profiles, Temperature Profiles and Angular Velocity Profiles

The effects of varying N^* on the velocity profiles, temperature profiles and angular velocity profiles against η are depicted in Figure 10. It is clear from the figures that the velocity profiles, temperature profiles and angular velocity profiles increase with an increase in N^*. We also observe that there is local maximum for velocity profiles and temperature profiles while angular velocity always decreases as η increases. Figure 10(a) illustrates velocity profiles, $u(0, \eta)$, against η for different values of the heat conduction parameter N^* (= 0.25, 0.50, 0.75, and 1.0). As N^* increases, the velocity profiles, $u(0, \eta)$, increase . In Figure 10(a), for all values of the heat conduction parameter N^*, there exists a local maximum of the velocity profiles, $u(0, \eta)$. These maximum values of the velocity profiles, $u(0, \eta)$, are 0.36891, 0.38174, 0.39588, and 0.411529 at $\eta = 1.53$ for $N^* = 0.5$,1.0, 1.5, and 2.0, respectively.

At $\eta = 1.53$, the velocity profile increases by 3.47, 7.31 and 11.55 percent, respectively, when N^* increases from 0.25 to 0.50, 0.75 and 1.0. Figure 10(b) also shows the temperature profiles, $\theta(0, \eta)$, against η for different values of the micropolar heat conduction parameter N^*(= 0.25, 0.50, 0.75, and 1.0). The temperature profiles decrease along η for all values of the heat conduction parameter N^*. Figure 10(c) depicts the angular velocity profiles, $N(0, \eta)$, against η for different values of the heat conduction parameter N^* (= 0.25, 0.50, 0.75 and 1.0). As N^* increases, the angular velocity profiles, $N(0, \eta)$, increase. In the same figure, it is seen that for all values of the heat conduction parameter N^*, there exists a local maximum of the angular velocity profiles, $N(0, \eta)$. These maximum values of the angular velocity profiles, $N(0, \eta)$, are 0.214790, 0.22260, 0.23209, and 0.24973 at $\eta = 1.83$ for $N^* = 0.25$, 0.50, 0.75, and 1.0, respectively. Again at $\eta = 1.83$, the angular velocity increases by 3.63, 8.05 and 12.07 percent, respectively, when N^* increases from 0.25 to 0.50, 0.75, and 1.0.

### 4.4. Effect of Vortex Viscosity Parameter, K on Transient Velocity Profiles, Temperature Profiles and Angular Velocity Profiles

Figure 11 exhibits the velocity profiles, temperature profiles and angular velocity profiles against η for different values of the vortex viscosity parameter, K. It is seen from the figure that the velocity profiles attain a maximum value while temperature profiles and angular velocity profile decrease monotonically with the increase of η. Figure 11(a) illustrates the velocity profiles, $u(0, \eta)$, against η for different values of the vortex viscosity parameter K (= 0.5, 1.0, 1.5, and 2.0). These figures display the effect of K on the velocity profiles, $u(0, \eta)$. As K increases, the velocity profiles, $u(0, \eta)$, increase. In the same figure, for each value of the vortex viscosity parameter K, there exists a local maximum of the corresponding velocity profile, $u(0, \eta)$. These maximum values of velocity profiles, $u(0, \eta)$, are 0.48234, 0.411529, 0.360379, and 0.322369 at $\eta = 1.56$ for $K = 0.5, 1.0, 1.5,$ and 2.0 respectively.

Also $\eta = 1.56$, the velocity profiles increases by 14.68, 25.28 and 33.16 percent, respectively, as K increases from 0.5 to 1.0, 1.5, and 2.0. Figure 11(b) shows temperature profiles, $\theta(0, \eta)$, against η for different values of the micropolar heat conduction parameter K (= 0.5, 1.0, 1.5, and 2.0). The temperature profile decreases along η for all values of the vortex viscosity parameter K. Figure 11(c) also depicts the angular velocity profile, $N(0, \eta)$, against η for different values of the vortex viscosity parameter K (= 0.5, 1.0, 1.5, and 2.0). As K increases, the angular velocity profile, $N(0, \eta)$, also increases. Finally, figure 11(c) shows that for every value of the vortex viscosity parameter, K, there exists a local maximum of the angular velocity profile, $N(0, \eta)$. These maximum values of the angular velocity profile, $N(0, \eta)$, are 0.27360, 0.24073, 0.214149, and 0.193509 at $\eta = 1.83$ for $K = 0.5, 1.0, 1.5,$ and 2.0, respectively. At $\eta = 1.83$, the angular velocity increases by 12.01, 21.72 and 29.27 percent, respectively, as K increases from 0.5 to 1.0, 1.5, and 2.0.
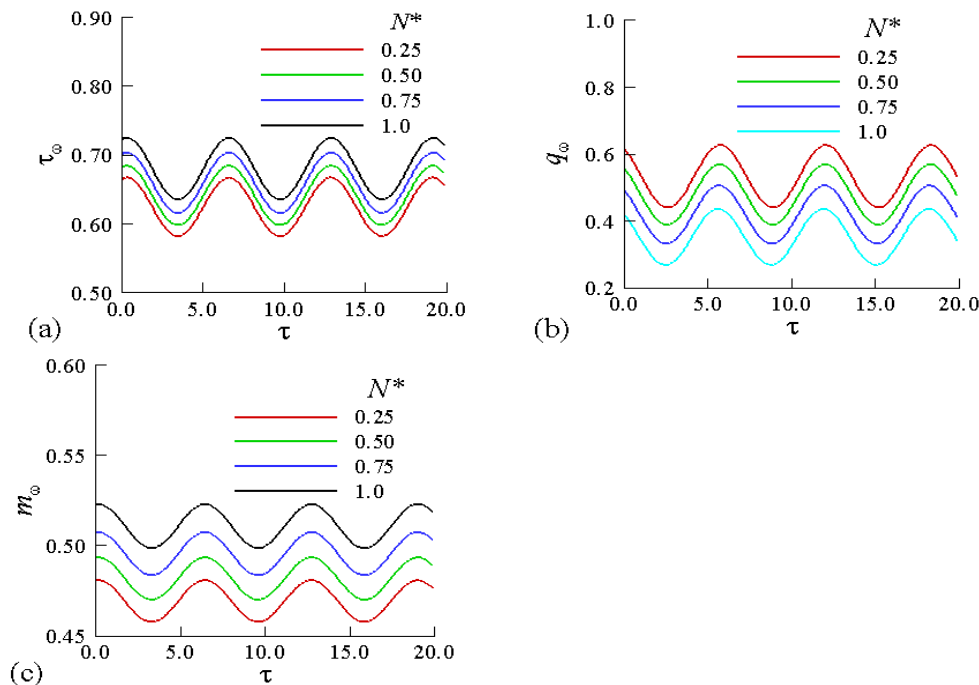

Figure 8. Numerical values of (a) surface shear stress (b) heat transfer coefficient and (c) couple-stress for different values of N^* against τ while $Pr = 9.0$ and $\omega = 1$
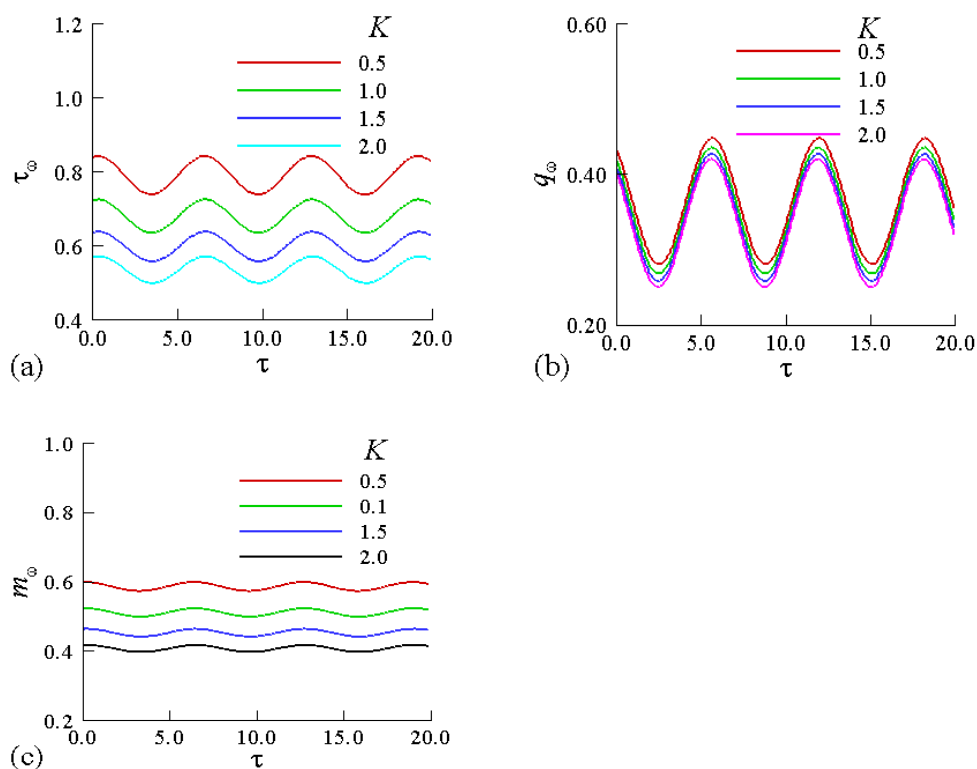
Figure 9. Numerical values of (a) shear stress (b) surface heat transfer coefficient and (c) couple-stress for different values of K against values of τ while $Pr = 9.0$ and $\omega = 1$
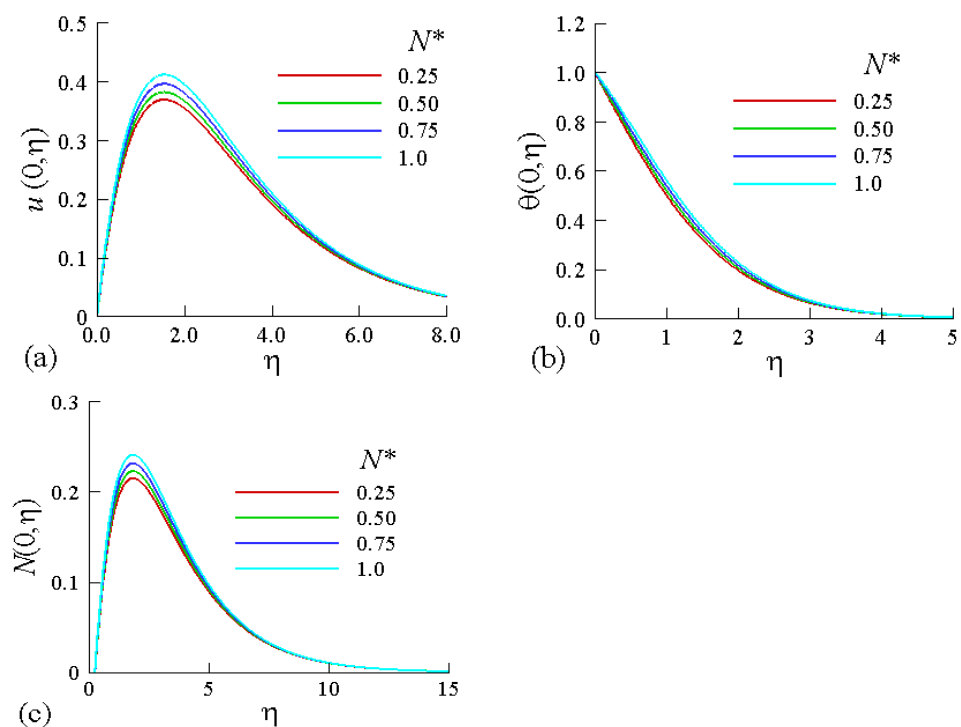
Figure 10. Numerical values of (a) velocity profiles (b) temperature profiles and (c) angular velocity profiles for different values of N^* against η while $Pr = 9.0$ and $\omega = 1$
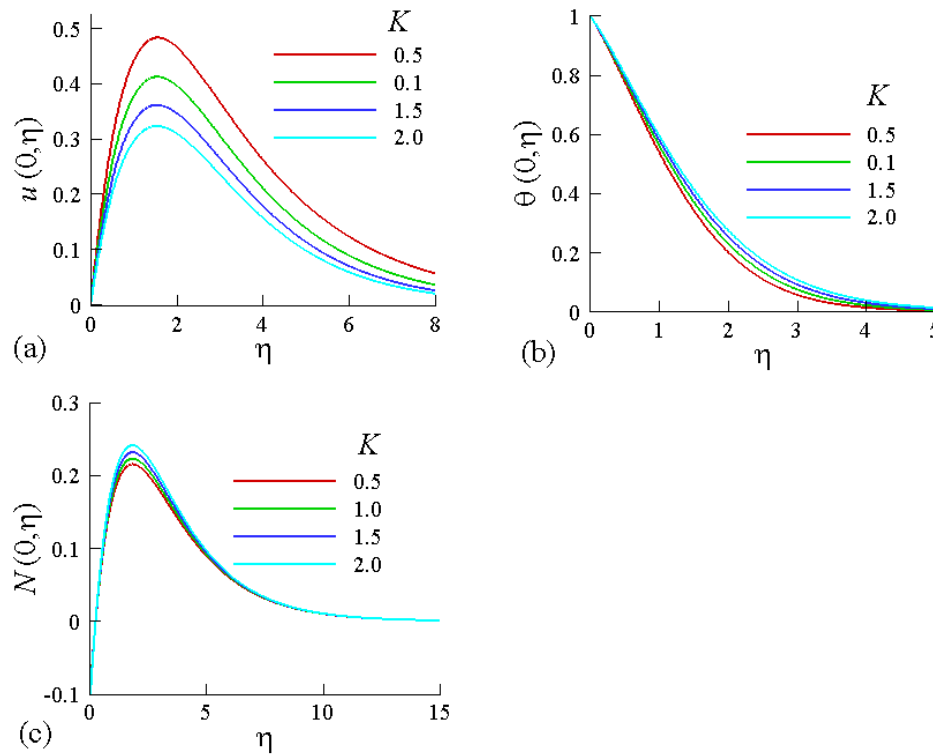
Figure 11. Numerical values of (a) velocity profiles (b) temperature profiles and (c) angular velocity profiles for different values of K against η while $Pr = 9.0$ and $\omega = 1$

5. Conclusions

In this paper, the unsteady free convection boundary layer flow of a thermo-micropolar fluid along a vertical plate has been discussed. It is assumed that the temperature of the plate is oscillating about a constant mean temperature, θ_w, with small amplitude, ε. The governing boundary layer equations are analyzed using, straight forward finite difference method for the entire values of locally varying variable, x. The effects of the material parameters such as angular velocity, N^*, the vortex viscosity parameter, K, on the shear stress, surface heat transfer and the couple-stress have been investigated. Through the present investigation it is found that micropolar fluids have a greater resistance (resulting from dynamic viscosity and vortex viscosity) to the fluid motion compared to Newtonian fluids.

REFERENCES

Ariman, T., Turk, M. A. and Sylvester, N. D. (1973). Microcontinum fluid mechanics-a review. Int. J. Eng. Sci., Vol. 11, pp. 905.

Ariman, T., Turk, M. A. and Sylvester, N. D. (1973). Application of microcontinum fluid mechanics. Int. J. Eng. Sci., Vol. 12, pp. 273.

Ahmadi, G. (1976). Self-similar solution of incompressible micropolar boundary layer flow over a semi-infinite plate. Int. J. Eng. Sci., Vol. 14, pp. 639.

Ashraf, M., Asghar, S and Hossain , M. A.(2012). Fluctuating hydromagnetic natural convection flow Past a magnetized vertical surface in the presence of thermal radiation. Thermal Sci., Vol. 16, pp.1081-1096.

Aziz, M. A. (2006), Thermal radiation effects on magnetohydrodynamic mixed convection flow of a micropolar fluid past a continuously moving semi-infinite plate for high temperature Differences. Acta Mechanica, Vol. 187, pp. 113–127.

Bhattacharyyaa, K., Mukhopadhyaya, S., Layek, G.C. Pop,I. (2012), Effects of thermal radiation on micropolar fluid flow and heat transfer over a porous shrinking sheet, Int. J. Heat Mass Transfer, Vol.55, pp. 2945–2952.

Chang, C.-L., Lee, Z.-Yi. (2008). Free convection on a vertical plate with uniform and constant heat flux in a thermally stratified micropolar fluid. Mech. Res. Comm., Vol. 35, pp.421–427.

Cheng, C. -Y., (2010). Nonsimilar solutions for double-diffusion boundary layers on a sphere in micropolar fluids with constant wall heat and mass fluxes. Appl. Math. Modelling Vol. 34, pp.1892–1900.

Cheng, C. –Y. (2008). Natural convection heat and mass transfer from a sphere in micropolar fluids with constant wall temperature and concentration, Int. Comm.   Heat   Mass Transfer, Vol.35, pp.750–755.

Chiu, C.-P., Chou, H.-M. (1993). Free convection in boundary layer flow of a micropolar fluid along a vertical wavy surface. Acta Mech., Vol. 101, pp. 161.

Eringen, A. C. (1966). Theory of micropolar fluids. J. Math. Mech., Vol. 16, pp. 1.

Eringen, A. C. (1972). Theory of thermomicrofluids. J. Math. Anal. Appl, Vol. 88, pp. 480–496.

Eshghy, S., Arpaci, V. S. and Clark, J. A. (1965). The effect of longitudinal oscillation on free convection from vertical surface. J. Appl. Mech. Vol.32, pp.183-191.

Gorla, R. S. R. (1983). Combined forced and free convection in micropolar boundary layer flow on a vertical flat plate. Int. J. Eng. Sci., Vol. 26, pp. 385.

Gorla, R. S. R. and Takhar, H. S. (1991). Unsteady mixed convection boundary layer flow of a micropolar fluid near the lower stagnation point on a cylinder. Int. J. Eng. Fluid Mech., Vol. 4, pp. 337–351.

Hadimoto, B. and Tokioka, T. (1969). Two-dimensional shear flows of linear micropolar fluids. Int. J. Eng. Sci., Vol. 7, pp. 515.

Helmy, K. A. (2000). State space approach to unsteady free convection flow of micropolar fluid. Acta Mech., Vol. 140, pp. 41−56.

Hossain, M. A., Chowdhury, M. K. and Takhar, H. K. (1995). Mixed convection flow of micropolar fluids with variable spin gradient viscosity along a vertical plate. J. Theo. Appl. Fluid Mech., Vol. 1, pp. 64.

Hossain, M. A., Das, S. K. and Pop, I. (1998a). Heat transfer response of mhd free Convection flow along a vertical plate To surface temperature oscillations. Int. J. Non-Linear Mech.Vol.33,pp. 541- 553.

Hossain, M. A., Das, S. K. and Rees, D. A. S., (1998b). Heat transfer response of free convection flow from a vertical heated plate to an oscillating surface heat flux. Acta Mechanica, Vol.126, pp.101-113.

Hossain, M. A., Chowdhury, M. K. and Gorla, R. S. R. (1999). Natural convection of thermomicropolar fluid from an isothermal surface inclined at a small angle to the horizontal. Int. J. Num. Meth. Heat and Fluid Flow, Vol. 9, pp. 814–832.

Hsiao, K. –L. (2010). Heat and mass transfer for micropolar flow with radiation effect past a nonlinearly stretching sheet. Heat Mass Transfer, Vol. 46, pp. 413–419.

Ishak, A., Nazar, R. Pop, I. (2008), Mixed convection stagnation point flow of a micropolar fluid towards a stretching sheet. Meccanica .Vol. 43, pp. 411– 418.

Ishak, A., Nazar, R, Pop, I.(2008). Magnetohydrodynamic flow of a micropolar fluid towards a stagnation point on a vertical surface. Comp. Math. Appl., Vol. 56, pp. 3188-3194.

Ishak, A. (2010), Thermal boundary layer flow over a stretching sheet in a micropolar fluid with radiation effect, Meccanica, Vol. 45, pp. 367–373.

Jaman, M. K. and Hossain, M. A. (2010). Effect of Fluctuating Surface Temperature on Natural Convection flow over cylinders of Elliptic Cross Section. Transport Phenomena Journal, Vol. 2, pp. 35-47.

Jena, S. K. and Mathur, M. N. (1981). Similarity solutions for laminar free convective flow of a thermomicropolar fluid past a non-isothermal vertical plate. Int. J. Eng. Sci., Vol. 19 (11), pp. 1431–1439.

Jena, S. K. and Mathur, M. N. (1982). Free convection in the laminar boundary layer flow of thermomicropolar fluid past a non-isothermal vertical plate with suction/injection. Acta Mech., Vol. 42, pp. 227–238.

Kelleher, M. D. and Yang, K. T. (1968). Heat transfer response of laminar free-convection boundary layers along a vertical heated plate to surface-temperature oscillations. J. App. Math. Phys., Vol. 19, pp. 31–44.

Kolpashchikov, V., Migun, N. P. and Prokhorenko, P. P. (1983). Experimental determinations of material micropolar coefficients. Int. J. Eng. Sci., Vol. 21, pp. 405.

Khonsari, M. M. and Brewe, D. (1989). On the performance of finite journal bearing lubricated wit micropolar fluids. STLE Tribology Trans., Vol. 32, pp. 155.

Lee, J. D. and Eringen, A. C. (1971). Boundary effects of orientation of nematic liquid crystals. J. Chem. Phys., Vol. 55, pp. 4509.

Lighthill, M. J. (1954). The response of laminar skin-friction and heat transfer to fluctuations in the stream velocity. Proc.. Royl. Soci.,Vol. A 224, pp. l-23.

Lockwood, F., Benchaita, M. and Freberg, S. (1987). Study of polyotropic liquid crystals in viscometric flow and elastohydrodynamic contact. ASLE Tribology Trans., Vol. 30, pp. 539.

Mathur, M. N. (1970). Laminar free convection flow of an elasticoviscous liquid from a non-uniformly heated vertical flat plate, Indian J. Pure Appl. Maths, Vol. 1, pp. 64–76.

Mahfouz, F.M. (2013). Numerical prediction of buoyancy driven micropolar fluid flow within uniformly heated eccentric annulus. Appl. Math. Modelling Vol.37, pp.6037–6054.

Muhuri, P. K. and Maiti, M. K. (1967). Free convection oscillatory flow from a horizontal plate. Int. Heat Mass Transfer, Vol.10, pp. 717-732.

Muri, Y. (1961). Buoyancy effects in forced laminar convection flow over a horizontal flat plate. J. Heat Transfer, Vol. 83, pp. 479.

Nanda, R. S. and Sharma, V. P. (1963). Free convection laminar boundary layers in oscillatory flow. J. Fluid Mech., Vol. 15, pp. 419-428.

Postelnicu, A. (2012). Free convection from a truncated cone subject to constant wall heat flux in a micropolar fluid. Meccanica, V0l. 47, pp.1349–1357.

Rees, D. A. S. and Bassom, P. Andrew (1996). The Blasius boundary-layer flow of a micropolar fluid. Int. J. Eng. Sci., Vol. 34, pp. 113–124.

Saleem, M., Asghar, S, Hossain, M.A. (2011). Natural convection flow of micropolar fluid in a rectangular cavity heated from below with cold sidewalls. Math. Comp Modelling, Vol.54, pp. 508–518.

Verma, R. L. (1982). Free convection fluctuating boundary layer on a horizontal plate. J. Appl. Math. Mech., Vol.63, pp.483-487.

Yacob, N. A. , Ishak , A., Pop , I. (2011) Melting heat transfer in boundary layer stagnation point flow towards a stretching/shrinking sheet in a micropolar fluid. Computers & Fluids, Vol. 47, pp. 16–21.

Yucel, A. (1989). Mixed convection micropolar fluid flow over horizontal plate with surface mass transfer. Int. J. Eng. Sci., Vol. 27, pp. 1593.